

Article

A Discontinuity-Capturing Methodology for Two-Phase Inviscid Compressible Flow

Jiratrakul Tunkeaw^a and Watchapon Rojanaratanangkule^{b,*}

Department of Mechanical Engineering, Faculty of Engineering, Chiang Mai University,
Chiang Mai 50200, Thailand

E-mail: ^ajiratrakul_earn@hotmail.com, ^{b,*}watchapon.roj@eng.cmu.ac.th (Corresponding author)

Abstract. The explicit filtering approach is applied to the quasi-conservative five-equation model of compressible two-phase flows to capture the interface between each fluid and a shock wave. The basic idea of the present filter is to combine a low-order linear filter with a high-order one via a proper discontinuity sensor and optimum linear weights. The capability of the proposed filter in capturing the contact discontinuity and damping the grid-to-grid oscillations is analysed. Various one-dimensional and two-dimensional test cases are performed, namely the interface advection of gas-gas flow, the shock-interface interaction, the gas-liquid Riemann problem, and the inviscid shock-bubble interaction. The numerical results reveal that the present filtering method can accurately capture the propagation of the shock waves and interfaces. Additionally, it produces less spurious oscillations compared with the existing 2nd-order discontinuity-capturing filter.

Keywords: Compressible two-phase flows, Euler's equation, explicit filtering, numerical oscillations, direct numerical simulation.

ENGINEERING JOURNAL Volume 25 Issue 11

Received 21 April 2021

Accepted 21 November 2021

Published 30 November 2021

Online at <https://engj.org/>

DOI:10.4186/ej.2021.25.11.45

1. Introduction

The main issue in conducting numerical simulations of fluid flow in the last several decades is the appearance of spurious oscillations. These occur due to the use of low-order central-difference schemes or the existence of a contact discontinuity. The oscillations owing to numerical schemes are normally eliminated by using dissipative (e.g. upwind schemes) or higher-order schemes. The discontinuity in variables, such as shock waves in compressible flows, high density ratio at the air-water interface, or high-pressure ratio in two-phase flows, also generates the grid-to-grid oscillations, generally called wiggles, while performing the spatial discretisation of the flow fields. These arise because the numerical schemes cannot capture the discontinuities in any variables. The wiggles are usually removed via the use of Total Variation Diminishing (TVD) [1], Essentially Non-Oscillatory (ENO) [2, 3] or Weighted ENO (WENO) [4, 5] schemes. The drawbacks of these methods are that they are quite difficult to be implemented into a computational fluid dynamics (CFD) solver and require a longer computational time compared to standard finite-difference or finite-volume schemes [6].

The grid-to-grid oscillations in all variables can also be removed to accurately capture shock waves via the use of explicit spatial filters and centred finite differences, as shown in the work of Bogey *et al.* [7]. These spatial filters are capable of reducing the numerical oscillations and capturing the steep interfaces, while increasing a little computational time. Although these filters work reasonably well for multi-species flows (i.e. different fluids having the same phase), the spurious oscillations still persist in the form of very small wiggles when applying the filters to two-phase flows, which have high-density and high-pressure ratios. Afterwards, Darian *et al.* [8] proposed a new shock-capturing method for a single-phase flow. Their filter utilises a low-order linear filter in the discontinuous region and a high-order linear filter in a smoother region. These filters are combined via nonlinear weights adjusting the amount of each filter. This method works very well in a single-phase flow. The wiggles are clearly removed from both regions, although it cannot correctly capture the steep interface. The interfaces are rather diffuse because the sensor of the filter cannot classify the discontinuous and the smooth regions well. A similar principle is also used by Beig & Johnsen [9] and Rodriguez & Johnsen [10] to develop a hybrid WENO scheme for multiphase compressible flow. The concept of the hybrid WENO scheme is to use a contact-discontinuity sensor [9, 10] based on pressure and density oscillations to distinguish between a discontinuous and a smooth region. Another different contact-discontinuity sensor is proposed

by Capuano *et al.* [11], referred to as a monotony indicator. This sensor is used to avoid damping in the absence of grid-to-grid oscillations similar to the concept of the hybrid WENO sensor, but it is easier to be implemented.

As mentioned earlier that there is no filtering approach that can well capture the discontinuity due to the interface between two fluids, the main objective of this research is to improve a filtering procedure for a simulation of two-phase compressible flow. The idea is to combine the monotony indicator of Capuano *et al.* [11] with the filtering methodology of Darian *et al.* [8] to capture a discontinuous interface and a shock wave without any spurious oscillations. The present filter is applied to an in-house direct numerical simulation (DNS) code with a multiphase-flow solver based on the concept of a volume-of-fluid (VOF) method.

2. Numerical Approach

The governing equations, discretisation methods and details of the present filter are presented below.

2.1. Governing Equations

In this work, the quasi-conservative five-equation model [12, 13, 14] is used to represent two-phase inviscid compressible flow. The governing equations written in a Cartesian coordinate system x_i are

$$\frac{\partial}{\partial t}(\rho_1\phi_1) + \frac{\partial}{\partial x_k}(\rho_1\phi_1u_k) = 0, \quad (1)$$

$$\frac{\partial}{\partial t}(\rho_2\phi_2) + \frac{\partial}{\partial x_k}(\rho_2\phi_2u_k) = 0, \quad (2)$$

$$\frac{\partial}{\partial t}(\rho u_i) + \frac{\partial}{\partial x_k}(\rho u_i u_k + p\delta_{ik}) = 0, \quad (3)$$

$$\frac{\partial}{\partial t}(\rho E) + \frac{\partial}{\partial x_k}(u_k[\rho E + p]) = 0, \quad (4)$$

$$\frac{\partial\phi_1}{\partial t} + u_k \frac{\partial\phi_1}{\partial x_k} = 0, \quad (5)$$

where $\rho_1\phi_1$ and $\rho_2\phi_2$ are respectively the phasic densities of phase 1 and 2, $\rho = \rho_1\phi_1 + \rho_2\phi_2$ is the mixture/total density, u_i is velocity vector, t denotes time and ϕ_1 is the volume fraction of phase 1. The total energy,

$$E = e + \frac{1}{2}u_i u_i, \quad (6)$$

is the summation of internal energy e and the kinetic energy. The closures of the system of equations are obtained with the stiffened gas equation of state (EOS) which has widely been utilized in two-phase compressible flow to describe pure gases and liquids [13, 15, 16]. Therefore, the relationship between the internal energy

e , temperature T and pressure p are given by [9]

$$\rho e = \frac{p}{\gamma - 1} + \frac{\gamma \pi_\infty}{\gamma - 1}, \quad \text{pressure-wise} \quad (7a)$$

$$\rho e = \rho c_v T + \pi_\infty, \quad \text{temperature-wise} \quad (7b)$$

where γ denotes the specific heat ratio and π_∞ is the fitting parameter [17, 18]. The specific heat at constant volume c_v is written in non-dimensional form as a function of a Mach number Ma as

$$c_v = \frac{1}{[\gamma(\gamma - 1)Ma^2]}. \quad (8)$$

The mixture rules (see, e.g., Beig & Johnsen [9]) are used to mix the individual fluid near the interface as,

$$\phi_1 + \phi_2 = 1, \quad (9)$$

$$\frac{1}{\gamma - 1} = \frac{\phi_1}{\gamma_1 - 1} + \frac{\phi_2}{\gamma_2 - 1}, \quad (10)$$

$$\frac{\gamma \pi_\infty}{\gamma - 1} = \frac{\gamma_1 \pi_{\infty,1}}{\gamma_1 - 1} \phi_1 + \frac{\gamma_2 \pi_{\infty,2}}{\gamma_2 - 1} \phi_2, \quad (11)$$

$$\pi_\infty = \pi_{\infty,1} \phi_1 + \pi_{\infty,2} \phi_2, \quad (12)$$

$$\rho c_v = \rho_1 \phi_1 c_{v,1} + \rho_2 \phi_2 c_{v,2}. \quad (13)$$

2.2. Spatial and Temporal Discretisations

The computations are performed by using an in-house DNS solver. All of the spatial derivatives are approximated via the use of a standard 4th-order central finite-difference scheme with a boundary treatment of Carpenter *et al.* [19]. The temporal advancement is obtained by an ultra-low-storage five-step 4th-order Runge-Kutta scheme [20]. An 11-point selective filter of Bogey *et al.* [21, 7] are used to enhance the stability of the numerical code. This selective filter is applied in order to reduce grid-to-grid oscillations, referred to as the Gibbs' oscillations. A discontinuity-capturing filter is then applied after the selective filter to capture shock waves and interfaces.

2.3. The Explicit Filtering Methodology

The idea of the present explicit filter is to combine the filtering approach of Darian *et al.* [8] with the monotony sensor of Capuano *et al.* [11]. A 2nd-order filter is employed to capture discontinuous interfaces and shock waves, while a 4th-order filter is applied in order to smooth variables in the far field. The present filter is applied at the end of each time step after utilising the 11-point selective filter to remove any grid-to-grid oscillations. The present filtering operation for a uniform grid is written as,

$$\tilde{U}_i = U_i - \left[d_1 \left(w_{i+\frac{1}{2}}^{(2)} D_{i+\frac{1}{2}}^{(2)} - w_{i-\frac{1}{2}}^{(2)} D_{i-\frac{1}{2}}^{(2)} \right) + d_2 \left(w_{i+\frac{1}{2}}^{(4)} D_{i+\frac{1}{2}}^{(4)} - w_{i-\frac{1}{2}}^{(4)} D_{i-\frac{1}{2}}^{(4)} \right) \right], \quad (14)$$

where \tilde{U}_i and U_i are respectively a filtered and non-filtered variable. The damping functions $D_{i\pm 1/2}^{(m)}$ at a cell interface is defined as

$$D_{i+\frac{1}{2}}^{(m)} = \sum_{j=1-n}^n c_j U_{i+j}, \quad D_{i-\frac{1}{2}}^{(m)} = \sum_{j=1-n}^n c_j U_{i+j-1} \quad (15)$$

where $n = 2$ for both of the 2nd-order ($m = 2$) and 4th-order filters ($m = 4$). The conservative coefficients c_j and the weighting factors d_1 and d_2 are given in Table 1.

	$m = 2$	$m = 4$
c_1	-1/4	-3/16
c_2	0	1/16
d_1	12/13	
d_2	1/13	

Table 1. The coefficients c_j for discontinuity-capturing filtering with $c_j = -c_{1-j}$ [11], and the weighting factors d_1 and d_2 .

The nonlinear weights $w_i^{(m)}$ are defined as a function of the discontinuity filtering strength σ_i in order to distinguish between the discontinuous and the smooth regions as

$$w_i^{(2)} = \sigma_i, \quad w_i^{(4)} = 1 - \sigma_i. \quad (16)$$

The weighting fluxes at the interface of two adjacent cells are then calculated as

$$w_{i+1/2}^{(m)} = 0.5(w_{i+1}^{(m)} + w_i^{(m)}), \quad (17a)$$

$$w_{i-1/2}^{(m)} = 0.5(w_i^{(m)} + w_{i-1}^{(m)}). \quad (17b)$$

The filtering strength used in Eq. (16) is defined as the maximum between the filtering intensity of the pressure and density fields

$$\sigma_i = \max(\sigma_i^p, \sigma_i^\rho). \quad (18)$$

The filtering strength of the pressure σ_i^p or density σ_i^ρ can be computed from

$$\sigma_i^{p/\rho} = \frac{M_i}{2} \left(1 - \frac{r_{th}}{r_s + \varepsilon} + \left| 1 - \frac{r_{th}}{r_s + \varepsilon} \right| \right). \quad (19)$$

The monotony indicator M_i and the discontinuity sensor r_s of the pressure and density are calculated from the procedure of Capuano *et al.* [11]. A threshold value of $r_{th} = 2 \times 10^{-5}$ is chosen throughout this work, while $\varepsilon = 10^{-16}$ is introduced to avoid numerical divergence.

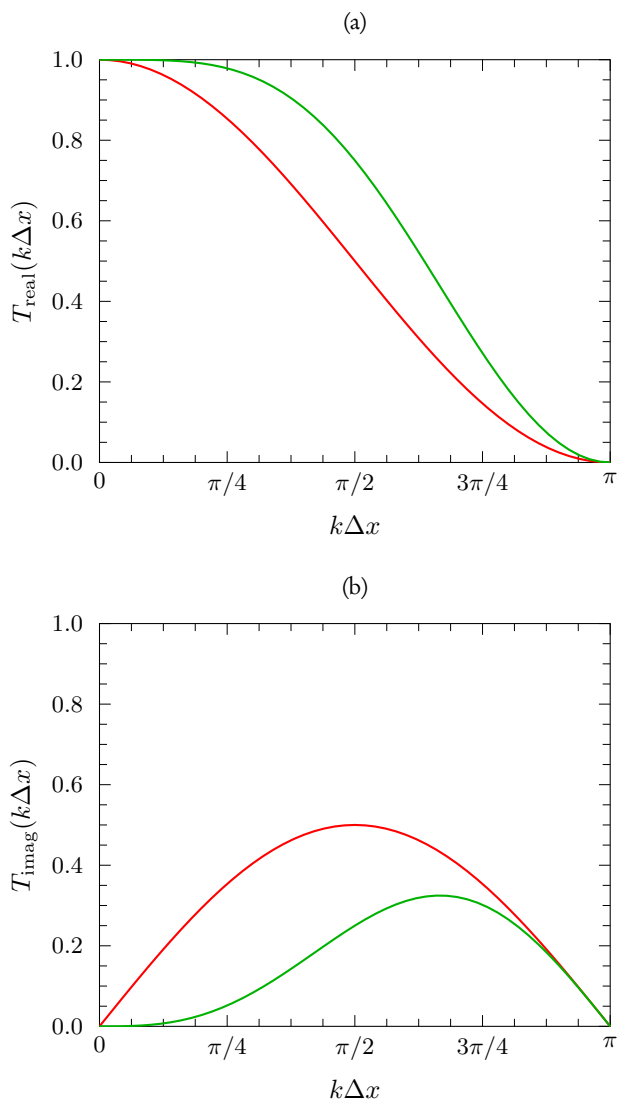


Fig. 1. Distribution of (a) the real part and (b) the imaginary part of the transfer function of the 2nd-order filter (—) and the 4th-order filter (—).

The transfer function of the 2nd-order and 4th-order linear filters are [7]

$$T_{\text{real}}(k\Delta x) = 1 + 2c_1 - 2 \sum_{j=1}^{n-1} (c_j - c_{j+1}) \cos(jk\Delta x) - 2c_n \cos(nk\Delta x), \quad (20a)$$

$$T_{\text{imag}}(k\Delta x) = -2 \sum_{j=1}^{n-1} (c_j + c_{j+1}) \sin(jk\Delta x) - 2c_n \sin(nk\Delta x). \quad (20b)$$

The real part of the transfer function illustrates how the filter attenuates the flow fields as a function of the wavenumber, while the imaginary part represents the phase errors of the filter. Since the present filter is constructed as a linear superposition of the 2nd-order and the 4th-order filters, its characteristics in the Fourier

space when both weights ($w_i^{(2)}$ and $w_i^{(4)}$) are not zero lie somewhere between the 2nd-order and 4th-order linear filters. Hence, it is expected that the present filter would yield better results than the discontinuity filter of Capuano *et al.* [11], where only the 2nd-order linear filter is employed. It is of importance to note that the linear weights d_1 and d_2 used in this work can change the transfer function profile of the filter. They are manually tuned with the constraint of $d_1 + d_2 = 1$.

3. Numerical Results

This section presents the numerical results of one-dimensional (1D) and two-dimensional (2D) test problems. These test problems are solved to study the capability and efficiency of the present filtering method. The numerical results are then compared with the discontinuity filter of Capuano *et al.* [11] and the exact solutions. Two different grid levels ($nx = 200$ and $nx = 1000$) are used for all the 1D test cases. For all of the simulations, the time step Δt is chosen in such a way that a maximum Courant–Friedrichs–Lewy (CFL) number is lower than 0.1.

3.1. Gas-Gas Interface Advection

The first test case is the advection of an interface between two gases in a periodic domain of size $-1 \leq x \leq 1$ [22, 23, 11]. The pressure and velocity of both gases are set to be constant and be the same. Hence, only the specific heat ratio and the density are discontinuous at the interface. The initial conditions are:

$$(\rho, u, p, \gamma) = \begin{cases} (1, 0.5, 1/1.4, 1.4), & \text{for } x \leq 0 \\ (10, 0.5, 1/1.4, 1.2), & \text{for } x > 0 \end{cases}. \quad (21)$$

The simulations are conducted until $t = 4$, when the flow returns to its initial position. Figure 2 shows the comparison between the numerical results using the present filter and the discontinuity filter of Capuano *et al.* [11] with the exact solution. The distribution of the mixture specific ratio γ and the total density ρ reveals that both filters can predict the interfaces at the correct locations (Figs. 2a and 2b), while the present filter seems to yield smoother interfaces. Once higher grid resolution is applied ($nx = 1000$), the interfaces predicted by both filter shift close to the exact solution, as shown in Fig. 2(e). From Figs. 2(c) and 2(d), it can be seen that the errors of velocity and pressure of both filters are about the same at the order of 10^{-15} .

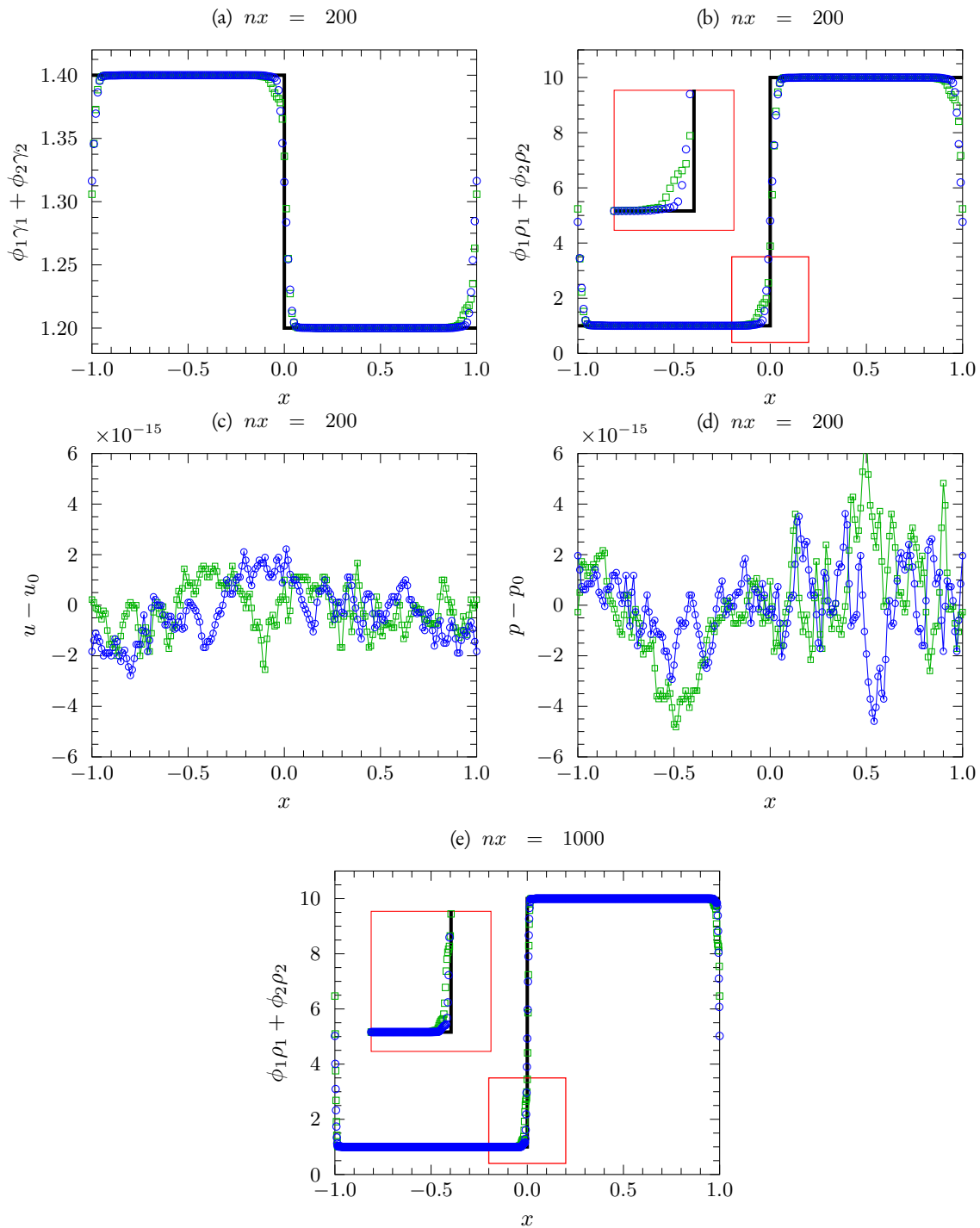


Fig. 2. Material interface advection of gas-gas flow at $t = 4$. The distribution of (a) mixture specific heat ratio γ , (b) total density ρ , (c) velocity error $u - u_0$, (d) pressure error $p - p_0$, and (e) total density using $nx = 1000$: — exact solution; \square 2nd-order filter of Capuano *et al.* [11]; \circ present filter.

3.2. Shock-Interface Interaction

This problem is concerned with a Mach 8.96 shock wave interacting with an interface [24]. At $t = 0$, the following conditions are used:

$$(\rho, u, p, \gamma) = \begin{cases} (0.386, 26.59, 100, 1.67), & \text{for } -1 \leq x < 0.8 \\ (0.1, -0.5, 1, 1.67), & \text{for } -0.8 \leq x < -0.2 \\ (1, -0.5, 1, 1.4), & \text{for } -0.2 \leq x \leq 1 \end{cases} \quad (22)$$

The numerical results of the shock-interface interaction problem are presented in Fig. 3. The computed results show a good agreement with the exact solution without large spurious oscillations in any variables. The mixture of specific heat ratio at the interface (indicated by the letter I) is rather smooth and is a little bit diffuse for both filters compared with the exact solution (Fig. 3a). Figure 3(b) presents a strong gradient of the mixture density field. It can be seen that both filters

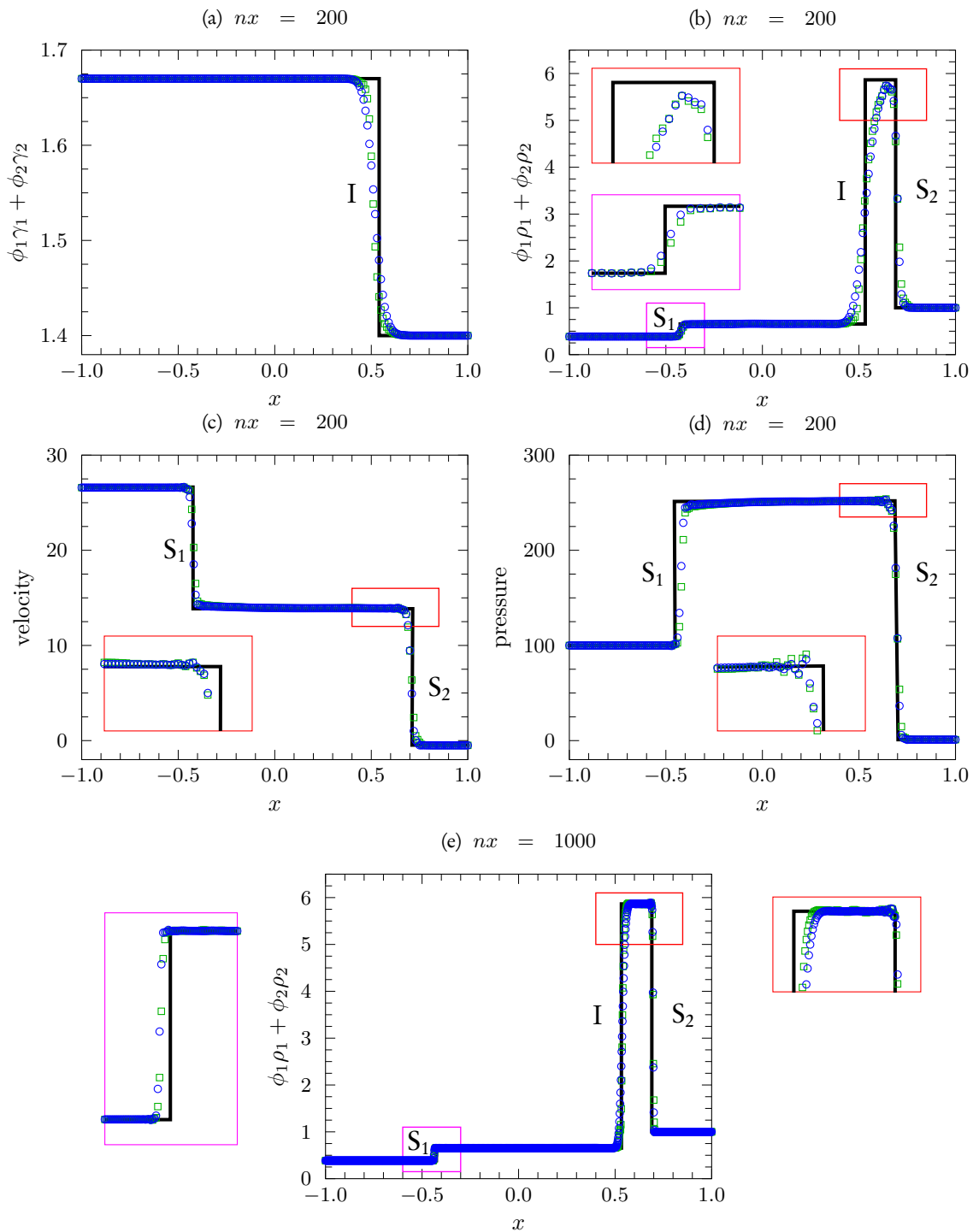


Fig. 3. Shock-interface interaction problem at $t = 0.07$. The profile of (a) mixture specific heat ratio γ , (b) total density ρ , (c) velocity u , (d) pressure p , and (e) Total density using $nx = 1000$: — exact solution; \square 2nd-order filter of Capuano *et al.* [11]; \circ present filter. The letters I, S_1 and S_2 indicate the interface, the upstream and downstream shock waves, respectively.

cannot perfectly capture both shock regions (denoted by the letters S_1 and S_2) of the mixture density field with $nx = 200$. Note that the shock S_1 is reflected backward, while the shock S_2 is transmitted into another fluid. Furthermore, the interface between each fluid of the density field is quite diffuse. On the other hand, the velocity and pressure distributions predicted by both filters are almost identical and agree well with the exact so-

lution, as shown in Figs. 3(c) and 3(d). Figure 3(e) shows that at higher-grid resolution ($nx = 1000$), the distribution of the total density exhibits very good agreement with the exact solution. Additionally, both filters are able to correctly capture the regions of the interface and the shock waves. It can be seen that the present filter is able to remove the small wiggles near both shock regions better than the filter of Capuano *et al.* [11].

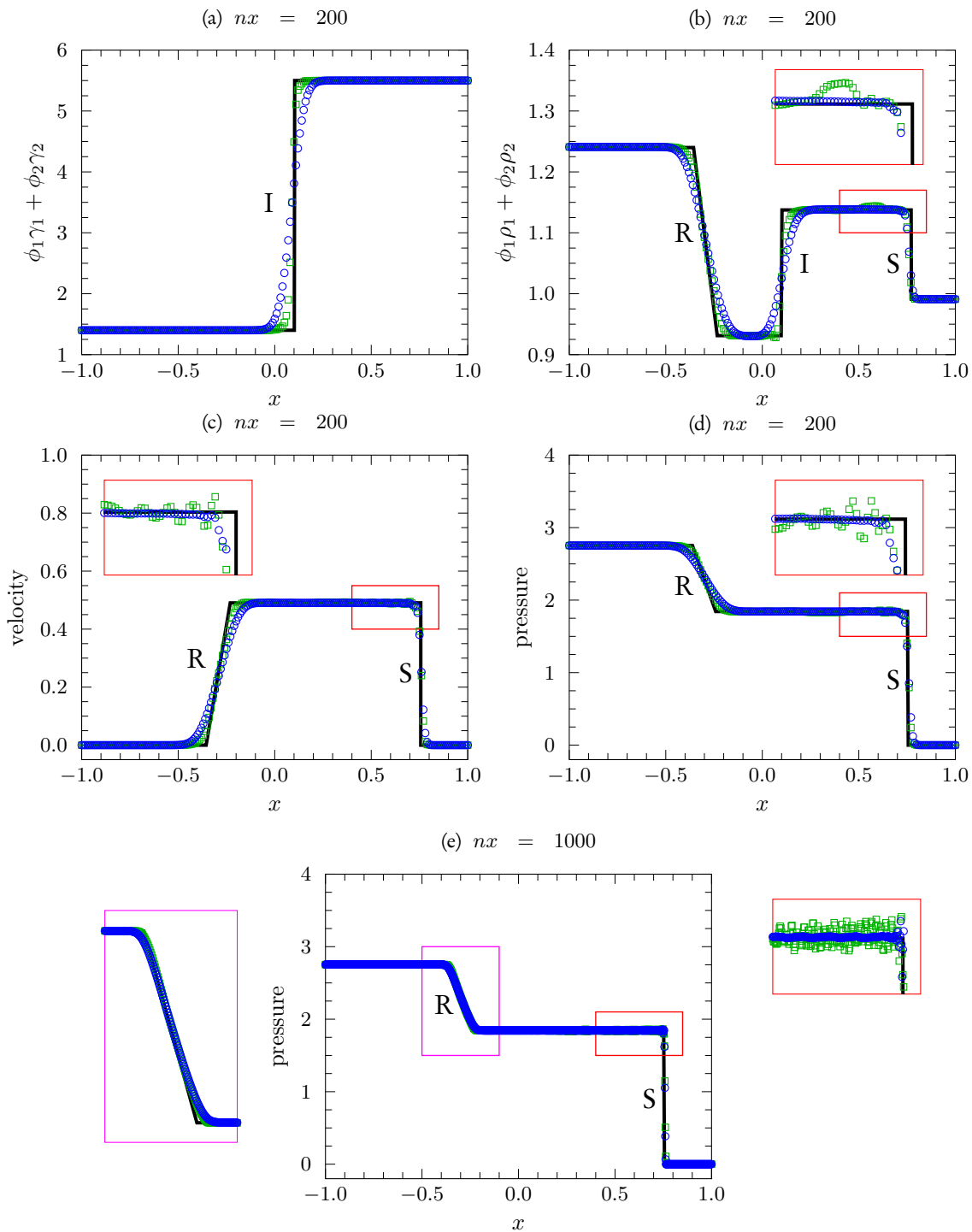


Fig. 4. Gas-liquid Riemann problem at $t = 0.2$. The profile of (a) mixture specific heat ratio γ , (b) total density ρ , (c) velocity u , (d) pressure p , and (e) pressure distribution using $nx = 1000$: — exact solution; \square 2nd-order filter of Capuano *et al.* [11]; \circ present filter. The letters I, R and S indicate the interface, the rarefaction wave and the shock wave, respectively.

3.3. Gas-Liquid Riemann Problem

For this 1D test case, the highly compressed gas that is generated by the high-pressure and low-density ratios of different phases is investigated. This problem is usually employed to mimic underwater explosions [25, 26]. The initial conditions in non-dimensional form are given by [22]:

$$(\rho, u, p, \gamma, \pi_\infty) = \begin{cases} (1.241, 0, 2.753, 1.4, 0), & \text{for } -1 \leq x < 0 \\ (0.991, 0, 3.059 \times 10^{-4}, 5.5, 1.505), & \text{for } 0 \leq x \leq 1 \end{cases} \quad (23)$$

Figure 4 presents the numerical results for the gas-liquid Riemann problem using two different filters. It

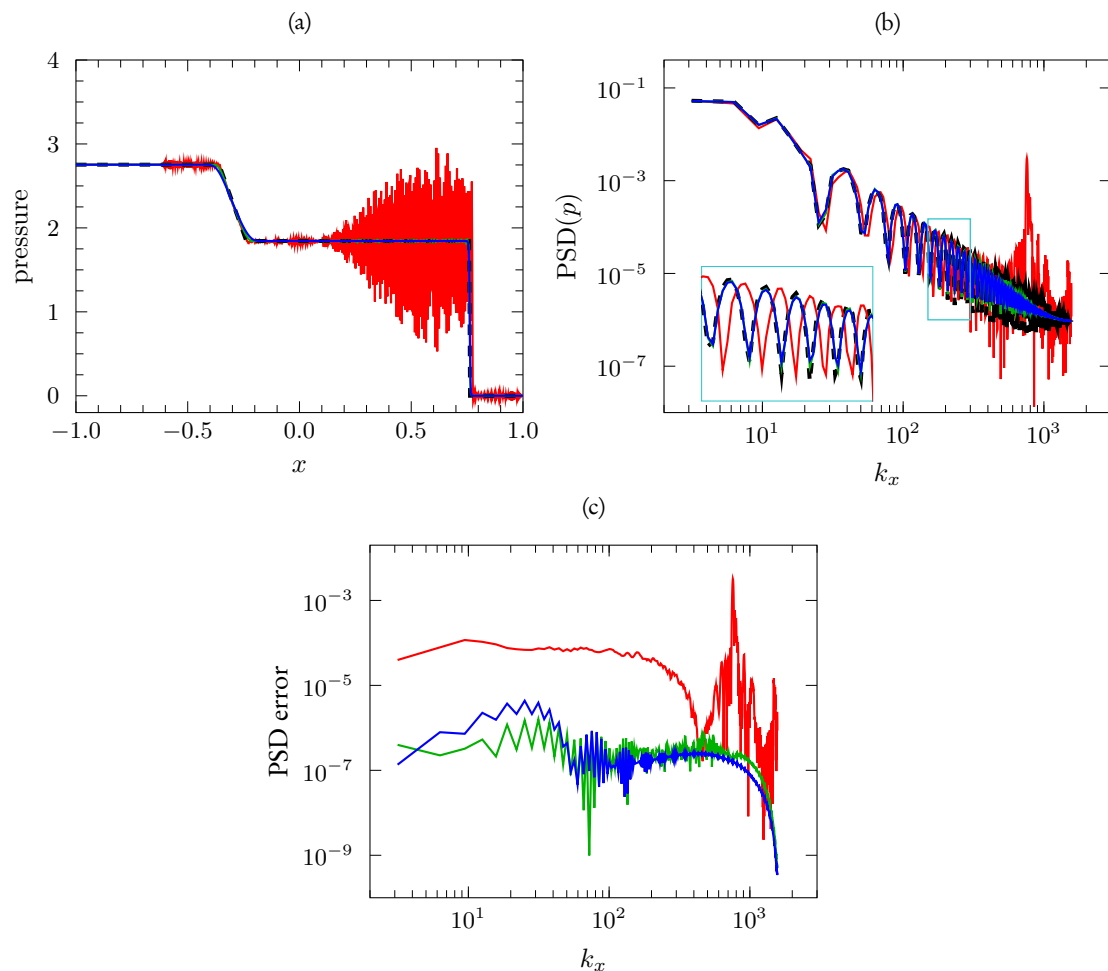


Fig. 5. Spectral analysis of gas-liquid Riemann problem using $nx = 1000$. (a) Pressure distribution, (b) its corresponding power spectral density (PSD) and (c) PSD error: --- exact solution; — no discontinuity-capturing filter; — 2nd-order filter of Capuano *et al.* [11]; — present filter.

can be seen that both filters can remove spurious oscillations very well. The mixture of specific heat ratio is well captured by both filters, although the interface region (denoted by the letter I) computed by the present filter is more diffuse than that of the filter of Capuano *et al.* [11] (Fig. 4a). It can be seen from Figs. 4(b) – 4(d) that a rarefaction wave (indicated by the letter R) propagating upstream is well captured by both filters. The location of the shock wave (denoted by the letter S) is correctly predicted by both filters, in spite of the appearance of the small wiggles close to the shock when the filter of Capuano *et al.* [11] is employed. The oscillations near the shock wave become stronger when higher grid resolution is employed, (Fig. 4e). In contrast, the rarefaction wave predicted by both filters looks identical and agrees very well with the analytical solution when using $nx = 1000$.

3.4. Filtering Spectral Analysis

The pressure distribution for the gas-liquid Riemann problem is chosen to analyse the capability of

the present explicit filter in removing the grid-to-grid oscillations. The oscillations usually arise at the high-gradient region and oscillate with high frequency, as shown in Fig. 5(a). The corresponding power spectrum density (PSD) of the pressure field is given in Fig. 5(b). These figures reveal that the use of filters not only gives good results in the physical space but their spectrum also fit well with the exact solution at low-wavenumber regions. At high-wavenumber regions, both filters are able to damp the PSD of the pressure field. This results in a reduction in the grid-to-grid oscillations that can be seen from all variables in the physical space, yielding a relatively smooth numerical data (see Fig. 4). The comparison between both filters in Fig. 5(b) also illustrates that the present filter has more efficiency in reducing the amplitude of the high-wavenumber parts. Figure 5(c) displays the power spectral error. The spectral error of the present filter is very small in the high-wavenumber regions. This confirms the capabilities of the present filter in removing the amplitude of the high-wavenumber parts in the wave space. However, the PSD error of the present filter is a little bit higher than that of the filter of

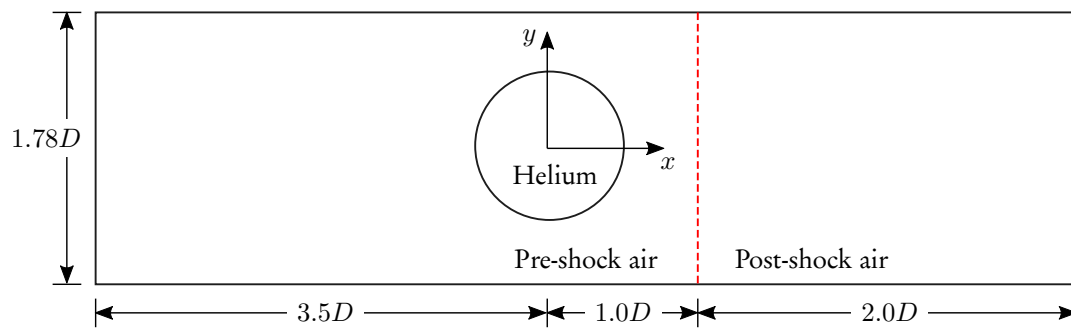


Fig. 6. Schematic and coordinate system of a 2D inviscid shock-bubble interaction problem.

Capuano *et al.* [11] at the low-wave number parts owing to the error from the diffuse interfaces and the smooth corners.

3.5. Two-Dimensional Inviscid Shock-Bubble Interaction

The present explicit filtering method is extended to a two-dimensional (2D) flow problem to test its capabilities in damping any spurious oscillations and capturing discontinuous interfaces, shock waves, and shear-layer instabilities. We consider an inviscid flow that consists of an air shock wave interacting with a helium bubble. This 2D inviscid problem of shock-bubble interaction has been numerically investigated by many researchers to test the efficiency of their discontinuity-capturing scheme [11, 23]. For this problem, the 2D computational domain is of size $[-3.5D, 3.0D] \times [-0.89D, 0.89D]$ with 2600×712 grid points in the streamwise (x) and the vertical (y) directions, respectively, as illustrated in Fig. 6. A helium bubble of diameter $D = 1.0$ is placed at location $[0.0D, 0.0D]$, while the air shock is launched at $x = 1.0D$ with the Mach number of 1.22. The initial conditions are

$$(\rho, u, v, p, \gamma) = \begin{cases} (1, 0, 0, 6.4637, 1.4), & \text{for pre-shock air} \\ (1.3764, -1, 0, 10.1482, 1.4), & \text{for post-shock air} \\ (0.1819, 0, 0, 6.4637, 1.648), & \text{for helium bubble} \end{cases} \quad (24)$$

The evolution of the helium bubble is visualised by the non-dimensional density gradient magnitude, $\phi = \exp(|\nabla\rho|/|\nabla\rho|_{\max})$, as shown in Fig. 7. The numerical results from the present filter are illustrated in the lower-half pictures and are compared with the simulation of Wong and Lele [23] (upper-half pictures of the left column), who employed the 5th-order weighted compact nonlinear scheme (WCNS5) with the 5th-order WENO-JS interpolation [5], and the results from the use of the 2nd-order filter of Capuano *et al.* [11] (upper-half pictures of the right column) at the same level of grid resolution. Initially ($t = 1.08$), all three methods yield qualitatively the same structures of the helium bubble, as depicted in Figs. 7(a) and 7(b). Once the helium

bubble convects further, small-scale features develop at the material interface due to interface instability. Since there is no physical dissipation in the governing equations, the capability of the numerical scheme to capture these small-scale structures only depend on its numerical dissipation. At $t = 1.64$, it can be seen from Figs. 7(c) and 7(d) that both filtering methods are not able to fully resolve all the small-scale structures that appear at the interface ($[x, y] \approx [2.0, \pm 0.2]$), although the shape of the bubble looks similar to that from the WCNS5-JS simulation [23]. Later at $t = 2.32$ (Figs. 7e and 7f), the present filter seems to be slightly better than the 2nd-order filter of Capuano *et al.* [11] in terms of producing small-scale features. However, the structure of the helium bubble predicted by both filters is quite different from that of Wong and Lele [23], due to the fact that both of the filtering methods possess higher numerical dissipation.

4. Conclusion

In order to eliminate the grid-to-grid oscillations that occur due to the existence of a contact discontinuity for compressible multiphase flow, the explicit filtering method is developed. It utilises a filtering approach of Darian *et al.* [8] together with the monotony indicator of Capuano *et al.* [11]. The present filter is applied to the quasi-conservative five-equation model to investigate its capability in capturing the high-gradient interfaces. The present filtering method is employed to simulate various test problems in both 1D and 2D. For the 1D test cases, the results are compared with the 2nd-order discontinuity filter of Capuano *et al.* [11] and the exact solution. The numerical results show that both filters can remove the numerical oscillations, even though the discontinuous interfaces are rather diffuse when compared with the exact solution. For the shock-interface interaction problem, both filters provide good results, although they require tremendous amount of grid resolution to correctly capture the interface region of the total density field. The present filter is more effective in terms of damping and removing the small oscillations than the filter of Capuano *et al.* [11], as can be clearly seen

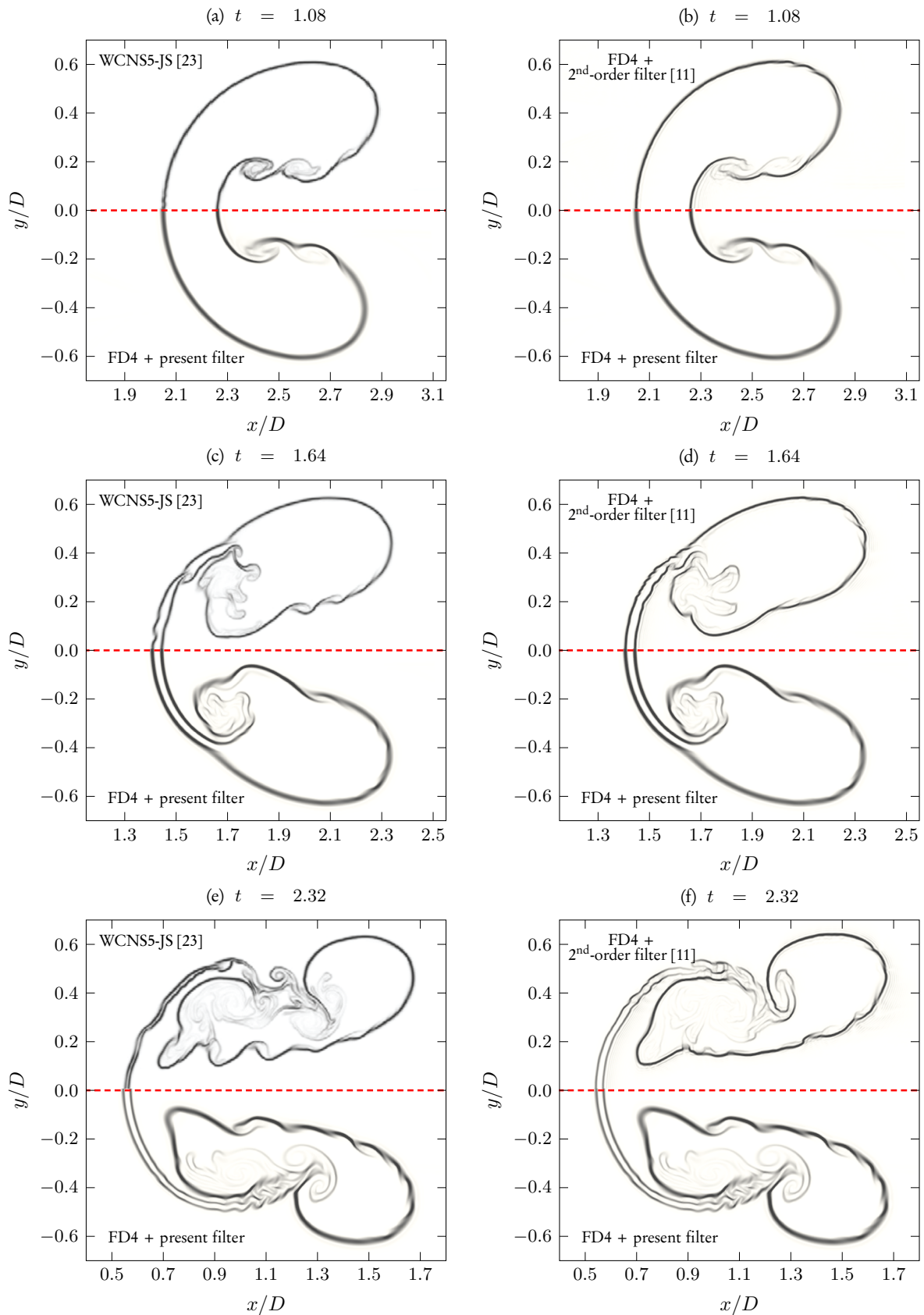


Fig. 7. Non-dimensional density gradient magnitude, $\phi = \exp(|\nabla\rho|/|\nabla\rho|_{\max})$, of the 2D inviscid shock-bubble interaction at $t = 1.08$ (top row), $t = 1.64$ (middle row), and $t = 2.32$ (bottom row). The left column shows the comparison of the results from the use of the present filter (lower-half pictures) with those from the WCNS5-JS method of Wong & Lele [23] (upper-half pictures), while the right column compares the results from the present filter (lower-half pictures) with those from the 2nd-order filter of Capuano *et al.* [11] (upper-half pictures).

from the gas-liquid Riemann test case. The power spectrum density of the pressure field from the gas-liquid Riemann problem is then analysed. The results show that the PSD of pressure from the use of both filters agrees well with the exact solution at low-wavenumber regions. For higher wavenumbers, both filters are able to damp the spurious oscillations. However, the present filter seems to be more effective in decreasing the amplitude of the PSD at the high-wavenumber parts, resulting in smaller PSD error at high-wavenumber regions. For the 2D shock-bubble interaction problem, the results from the present filter and the 2nd-order filter of Capuano *et al.* [11] are almost identical, even though they look different from the WCNS5-JS simulation of Wong and Lele [23]. This is because both filtering methods have less capability in resolving small-scale structures due to possessing higher numerical dissipation than a WENO-type scheme.

Acknowledgement

This work is supported by the scholarships from the Graduate School and the Faculty of Engineering, Chiang Mai University.

References

- [1] A. Harten, "High resolution schemes for hyperbolic conservation laws," *J. Comput. Phys.*, vol. 49, no. 3, pp. 357–393, 1983.
- [2] A. Harten, B. Engquist, S. Osher, and S. R. Chakravarthy, "Uniformly high order accurate essentially non-oscillatory schemes, III," *J. Comput. Phys.*, vol. 71, no. 2, pp. 231–303, 1987.
- [3] C.-W. Shu and S. Osher, "Efficient implementation of essentially non-oscillatory shock-capturing schemes," *J. Comput. Phys.*, vol. 77, no. 2, pp. 439–471, 1987.
- [4] X.-D. Liu, S. Osher, and T. Chan, "Weighted essentially non-oscillatory schemes," *J. Comput. Phys.*, vol. 115, no. 1, pp. 200–212, 1994.
- [5] G.-S. Jiang and C.-W. Shu, "Efficient implementation of weighted eno schemes," *J. Comput. Phys.*, vol. 126, no. 1, pp. 202–228, 1996.
- [6] E. Johnsen, J. Larsson, A. V. Bhagatwala, W. H. Cabot, P. Moin, B. J. Olson, P. S. Rawat, S. K. Shankar, B. Sjögren, H. C. Yee, X. Zhong, and S. K. Lele, "Assessment of high-resolution methods for numerical simulations of compressible turbulence with shock waves," *J. Comput. Phys.*, vol. 229, no. 4, pp. 1213–1237, 2010.
- [7] C. Bogey, N. de Cacqueray, and C. Bailly, "A shock-capturing methodology based on adaptive spatial filtering for high-order non-linear computations," *J. Comput. Phys.*, vol. 228, no. 5, pp. 1447–1465, 2009.
- [8] H. M. Darian, V. Esfahanian, and K. Hejranfar, "A shock-detecting sensor for filtering of high-order compact finite difference schemes," *J. Comput. Phys.*, vol. 230, no. 3, pp. 494–514, 2011.
- [9] S. A. Beig and E. Johnsen, "Maintaining interface equilibrium conditions in compressible multiphase flows using interface capturing," *J. Comput. Phys.*, vol. 302, pp. 548–566, 2015.
- [10] M. Rodriguez and E. Johnsen, "A high-order accurate five-equations compressible multiphase approach for viscoelastic fluids and solids with relaxation and elasticity," *J. Comput. Phys.*, vol. 379, pp. 70–90, 2019.
- [11] M. Capuano, C. Bogey, and P. D. M. Spelt, "Simulations of viscous and compressible gas-gas flows using high-order finite difference schemes," *J. Comput. Phys.*, vol. 361, pp. 56–81, 2018.
- [12] G. Allaire, S. Clerc, and S. Kokh, "A five-equation model for the simulation of interfaces between compressible fluids," *J. Comput. Phys.*, vol. 181, no. 2, pp. 577–616, 2002.
- [13] D. P. Garrick, M. Owkes, and J. D. Regele, "A finite-volume HLLC-based scheme for compressible interfacial flows with surface tension," *J. Comput. Phys.*, vol. 339, pp. 46–67, 2017.
- [14] D. P. Garrick, W. A. Hagen, and J. D. Regele, "An interface capturing scheme for modeling atomization in compressible flows," *J. Comput. Phys.*, vol. 344, pp. 260–280, 2017.
- [15] S. Osher and R. P. Fedkiw, "Level set methods: An overview and some recent results," *J. Comput. Phys.*, vol. 169, no. 2, pp. 463–502, 2001.
- [16] V. Coralic and T. Colonius, "Finite-volume WENO scheme for viscous compressible multi-component flows," *J. Comput. Phys.*, vol. 274, pp. 95–121, 2014.
- [17] O. Le Métayer, J. Massoni, and R. Saurel, "Modelling evaporation fronts with reactive Riemann solvers," *J. Comput. Phys.*, vol. 205, no. 2, pp. 567–610, 2005.
- [18] M. Aslani and J. D. Regele, "A localized artificial diffusivity method to simulate compressible multiphase flows using the stiffened gas equation of

- state,” *Int. J. Numer. Methods Fluids*, vol. 88, no. 9, pp. 413–433, 2018.
- [19] M. H. Carpenter, J. Nordström, and D. Gottlieb, “A stable and conservative interface treatment of arbitrary spatial accuracy,” *J. Comput. Phys.*, vol. 148, no. 2, pp. 341–365, 1999.
- [20] C. A. Kennedy, M. H. Carpenter, and R. M. Lewis, “Low-storage, explicit Runge–Kutta schemes for the compressible Navier–Stokes equations,” *Appl. Numer. Math.*, vol. 35, no. 3, pp. 177–219, 2000.
- [21] C. Bogey and C. Bailly, “A family of low dispersive and low dissipative explicit schemes for flow and noise computations,” *J. Comput. Phys.*, vol. 194, no. 1, pp. 194–214, 2004.
- [22] E. Johnsen and T. Colonius, “Implementation of WENO schemes in compressible multicomponent flow problems,” *J. Comput. Phys.*, vol. 219, no. 2, pp. 715–732, 2006.
- [23] M. L. Wong and S. K. Lele, “High-order localized dissipation weighted compact nonlinear scheme for shock- and interface-capturing in compressible flows,” *J. Comput. Phys.*, vol. 339, pp. 179–209, 2017.
- [24] E. Johnsen, “Numerical simulations of non-spherical bubble collapse with applications to shockwave lithotripsy,” Ph.D. dissertation, California Institute of Technology, Pasadena, USA, 2007.
- [25] J. P. Cocchi, R. Saurel, and J. C. Loraud, “Treatment of interface problems with Godunov-type schemes,” *Shock Waves*, vol. 5, pp. 347–357, 1996.
- [26] K.-M. Shyue, “An efficient shock-capturing algorithm for compressible multicomponent problems,” *J. Comput. Phys.*, vol. 142, no. 1, pp. 208–242, 1998.



Jiratrakul Tunkeaw is a Ph.D. student in the Department of Mechanical engineering, Faculty of Engineering, Chiang Mai University, Thailand. He also obtained M.Eng. and B.Eng. in Mechanical Engineering from Chiang Mai University. He has experience in Computational Fluid Dynamics (CFD), numerical programming, and turbulence simulation.



Watchapon Rojanaratanangkule is an Assistant Professor in the Department of Mechanical Engineering, Chiang Mai University. He obtained his Ph.D. in the area of computational and theoretical fluid dynamics from the University of Southampton. His research interest includes high-performance computing (HPC), high-order accurate numerical algorithms, vortex dynamics, compressible flows, aeroacoustics, hydrodynamic instabilities, and turbulence. He has published several articles in refereed journals and conference proceedings.